Handling Editor: Sanzhong Li

Journal Pre-proof

Zircon U-Pb geochronology of the Chimpa volcano (Central Andes, Puna plateau, NW Argentina): Inferences on the temporal evolution of the magmatic system

E. Bustos , L. Bardelli , M. Arnosio , R.A. Becchio

PII: S2772-8838(23)00060-2
DOI: https://doi.org/10.1016/j.geogeo.2023.100237
Reference: GEOGEO 100237

To appear in: *Geosystems and Geoenvironment*

Received date: 2 August 2023
Revised date: 28 August 2023
Accepted date: 20 September 2023

Please cite this article as: E. Bustos , L. Bardelli , M. Arnosio , R.A. Becchio , Zircon U-Pb geochronology of the Chimpa volcano (Central Andes, Puna plateau, NW Argentina): Inferences on the temporal evolution of the magmatic system, *Geosystems and Geoenvironment* (2023), doi: https://doi.org/10.1016/j.geogeo.2023.100237

Highlights

- Zircon U-Pb ages indicate a lifespan for Chimpa volcanism ranging 7.5 to <7.0 Ma.
- Zircon crystallization at high magmatic temperatures from poorly evolved melts.
- Juxtaposition of accessory antecrysts in the pre-eruptive melts.
- Magmatic ages are concordant with a steady-state magmatic phase of the Puna.

Zircon U-Pb geochronology of the Chimpa volcano (Central Andes, Puna plateau, NW Argentina): Inferences on the temporal evolution of the magmatic system

E. Bustos*, L. Bardelli, M. Arnosio, R.A. Becchio

IBIGEO– CONICET – Universidad Nacional de Salta, Av. Bolivia 5150, A4400FVY, Salta, Argentina

*Corresponding author. E-mail address: emilcebustos@gmail.com

Handling Editor: Sanzhong Li

Abstract

We investigated the temporal evolution of the andesitic Chimpa volcano of the northern Puna plateau, Central Andes, situated at the geological boundary between the plateau and the Eastern Cordillera domains. The volcanic activity consisted in three constructive volcanic cycles (Basal, Cajon, and Chimpa units) showing complex eruptive behaviors (ignimbrites, lava domes. block-and-ash flows, lava flows). We present new U-Pb analyses conducted on the zircon crystals from the Chimpa volcanic rocks. These analyses provide constraints on the magmatic/volcanic tempos and offer insights into the Th and U (and Th/U ratios) systematics of the analyzed zircon crystals. The results suggest a lifespan for volcanism ranging 7.5 to <7.0 Ma, in concomitance with the regional steady-state magmatic phase separating the first two pulses of ignimbritic flare-up in the Altiplano-Puna Volcanic Complex. Moreover, the analyzed zircon crystals exhibit Th/U ratios (0.11-0.34) and Th (33-8860 ppm) and U (52-4258 ppm) that indicate magmatic crystallization from poorly evolved melts at high temperatures. Some discrepancies exist between the calculated zircon concordia age for the third volcanic phase (Chimpa Unit, ca. 7.35 ± 0.071 Ma) and that of the second cycle (Cajon Unit, 6.98 ± 0.057 Ma).

We interpret these differences as stemming from the presence of zircon antecrysts in the final eruptive melts. Indeed, a true pre-eruptive event of zircon crystallization (i.e., formation of autocrysts) could not be proven by the existing dataset.

There is a geochronological affinity with some nearby volcanic rocks from the Puna plateau and the Eastern Cordillera domains, particularly considering the rhyolitic products of the Ramadas Volcanic Center and the andesitic to dacitic Almagro volcanic rocks. This highlights the complex behavior of the local magma plumbing system beneath this particular area, resulting in the emission of geochemically variegate volcanic rocks at similar times. This scenario suggests that the composition of the erupting melts are affected by the rheological behavior of the mid-upper-crustal MASH reservoir (the Altiplano-Puna Magmatic Body), which may either facilitate or impede the ascent of poorly evolved magmas derived from the deep crust towards the surface. From this point of view, the relative location of the volcanic centers relatively to the position of the geophysical anomaly may exert an important influence on the petrogenetic paths of magmas.

Keywords: Puna plateau; Steady-state magmatism; Zircon Th/U; Zircon U-Pb ages

1. Introduction

The Central Andes are one of the most important volcanic zones on Earth, encompassing the Altiplano-Puna Volcanic Complex (referred to as APVC), a prominent site of ignimbritic flare-up activity in the Puna plateau of northern Chile and Argentina during approximately 10-1 million years (de Silva, 1989). The U-Pb chronostratigraphy of zircon from volcanic rocks has revealed the occurrence of pulses of high-flux magmatism interspersed with periods of low-flux, steady-state volcanism (de Silva et al., 2015; Kern et al., 2016). Geophysical data point to a regional, mid-crustal, partially molten zone beneath the APVC, known as the Altiplano-Puna Magmatic Body (referred to as APMB; Zandt et al., 2003; Ward et al., 2014). Additionally, a

smaller geophysical anomaly is recognized beneath a restricted area at the boundary between the northern Puna and Eastern Cordillera domains (Zandt et al., 2003). This area has witnessed varied volcanic activity from the Late Miocene to recent times (e.g., Viramonte et al., 1984; Coira et al., 1993; Petrinovic et al., 1999, 2006; Matteini et al., 2002; Mazzuoli et al., 2008; Maro et al., 2017; Coira et al., 2018; Escudier-Viruete et al., 2022). Existing geochronological studies indicate that volcanism in this area has predominantly occurred since the Late Miocene (e.g., Petrinovic et al., 1999; Matteini et al., 2002; Mazzuoli et al., 2008). However, studies specifically focusing on the U-Pb systematics of volcanic zircons offer only a partial perspective of the volcanic history of this region (e.g., Hongn et al., 2002; Lucci et al., 2018; Bardelli et al., 2021).

In this study, our focus is on the timeline of the late miocenic Chimpa composite volcano of northern Puna (Fig. 1; Arnosio, 2010; Norini et al., 2013; Bustos et al., 2020, 2022). We considered the zircon population contained within the volcanic rocks, being this mineral one of the most efficient in tracking the temporal evolution of magmatic and volcanic systems (e.g., Balaram et al., 2022; Chakraborty et al., 2022; Lucci et al., 2018). We present new U-Pb age determinations on zircon coupled with the Th and U chemical characterization, aiming to achieve the following objectives: (i) contributing to the U-Pb chronostratigraphic record of this sector of the Puna plateau, (ii) constraining the timing of the magmatic and/or volcanic activity of the Chimpa volcano, and (iii) exploring the evolution of the local magmatic context. The results provide valuable insights into the lifespan of the magmatic system linked to this volcano and allow improving our understanding of the magmatic context of the Chimpa area and its surroundings during the Late Miocene.

2. Geological background

2.1. Regional geology

Volcanism in the Central Andes results from the subduction of the Nazca plate beneath South America (e.g., James, 1971). A principal volcanic sector of the Andean Cordillera is the Altiplano-Puna, a broad plateau that comprehends some of the most voluminous caldera-forming ignimbrites on Earth (de Silva, 1989; Lindsay et al., 2001; Schmitt et al., 2002). These volcanic deposits are the result of high-flux magma regimes (flare-up) characterizing the APVC from the late Miocene to the Pleistocene (ca. 10-1 Ma). In this context, four main pulses of ignimbritic eruptions (lasting 2-3 Ma) alternated with periods of lower, "normal" magma flux from the mantle source (steady-state regime; de Silva et al., 2015; Kern et al., 2016; Wörner et al., 2018; de Silva and Kay, 2018) are recognized. At depth, the prominent geophysical anomaly of the APMB is thought to represent a partially-molten, mid-crustal (25-15 km depth), MASH (melting, assimilation, storage, homogenization; after Hildreth and Moorbath, 1988) region (Chmielowski et al., 1999; Zandt et al., 2003; Ward et al., 2014). Towards the SE of the APVC area, close to the geological boundary between the Puna plateau and the Eastern Cordillera of NW Argentina, an apophysis of the main APMB is recognized, as indicated by Zandt et al. (2003; Fig. 1b). The Chimpa magma system developed within this region.

This sector of the plateau is characterized by an important fault system known as the Calama-Olacapato-El Toro (COT; e.g., Viramonte et al., 1984; Salfity, 1985; Matteini et al., 2002; Giordano et al., 2013). This is a major segment of crustal deformation spanning approximately 300 km in length and with a maximum width ranging 10-20 km (e.g., Allmendinger et al., 1983; Acocella et al., 2011; Norini et al., 2013). The COT acts as a boundary dividing the southern and the northern Puna regions (Alonso et al., 1984) and served as a primary transfer zone for deformation and magmas in the Puna back-arc (e.g., Norini et al., 2013). The COT area hosts a diversified suite of volcanic structures, including big calderas, composite volcanoes and lava domes of intermediate composition, rhyolitic centers, and mafic monogenetic volcanoes (Fig. 1b; e.g., Viramonte et al., 1984; Coira et al., 1993; Petrinovic et al., 1999, 2010; Coira and Cisterna, 2021). The late miocenic volcanic activity in the area

includes the Aguas Calientes and Negra Muerta calderas (Petrinovic et al., 2005, 2010), the Quevar and Chimpa volcanoes (Robl et al., 2009; Escudier-Viruete et al., 2022; Arnosio, 2010; Bustos et al., 2020), the dacitic El Morro lava dome (Petrinovic et al., 1999), and the rhyolitic Ramadas Volcanic Center (Viramonte et al., 1984; Lucci et al., 2018; Coira et al., 2018). Additionally, magmatic (monzogabbros to monzogranites) and volcanic (andesites and dacites) rocks are also reported in the Eastern Cordillera domain (Mazzuoli et al., 2008). In the study area, the basement lithologies are predominantly composed by Late Neoproterozoic and Lower Paleozoic metasedimentary sequences, along with Cretaceous–Neogene sedimentary units (e.g., Turner, 1964; Ramos, 1970; Ramos, 1973; Aceñolaza and Aceñolaza, 2005; del Papa and Petrinovic, 2017).

2.2. The Chimpa volcano

The Chimpa volcano is located in the Puna plateau of northwest Argentina, approximately 40 km north of the COT lineament and at the boundary between the Puna plateau and the Eastern Cordillera domains (Fig. 1a, b). It crops out in the western side of the San Antonio de los Cobres range, a depression bounded by N-S inverse faults that are thought to control the emplacement depth of the local upper-crustal magma reservoirs (Norini et al., 2013; Fig. 1b).

The Chimpa volcanic deposits show an asymmetric radial pattern that extends northward and westward from the eruptive center (Arnosio, 2010; Fig. 1c; Fig. 2a). As proposed by Arnosio (2002, 2010) and Bustos et al. (2020), the volcanic stratigraphy of the Chimpa volcano is defined (from the base to the top) by three discrete units representing eruptive cycles: (i) the Basal Unit, characterized by pyroclastic density currents, (ii) the Cajon Unit, consisting of lava domes and associated block-and-ash flow deposits, and (iii) the Chimpa Unit, characterized predominantly by lava flows. The volcanic evolution culminates with the collapse of the volcanic edifice (Casana Unit; Fig. 1c; Norini et al., 2020; Bustos et al., 2020, 2022).

Below we describe the main lithologic and petrographic features of the Chimpa lithologies (following Arnosio, 2010 and Bustos et al., 2020).

2.2.1. Basal Unit

The Basal Unit comprises a sub-horizontal, massive, moderately consolidated ignimbrite sheet with approximately 30 m of thickness (Fig. 2b). The deposits consist of varying proportions of pumiceous and lithic fragments embedded in a tuff matrix with plagioclase, biotite, hornblende, opaque minerals, and glass shards. Pumice fragments are defined, in order of abundance, in white, gray and banded types. The white pumice clasts display moderate crystal content, comprising 20-30% of plagioclase, biotite, and hornblende (Fig. 3a; Table 1). The gray pumice are crystal-rich (approximately 50% of crystals; Table 1) and occur both as isolated fragments within the ignimbrite and as inclusion within the white pumice. They display a phenocryst association of hornblende, biotite, plagioclase, and opaque minerals (Fig. 3b). The banded pumice clasts present a layered structure, with alternating bands of both white and gray pumice. A paraconformity separates the Basal Unit from the upper Cajon Unit, indicating an important change in the eruptive style (Bustos et al., 2020).

2.2.2. Cajón Unit

The Cajón Unit consists of coherent effusive (lava domes) and pyroclastic (block-and-ash flow) deposits with maximum thickness of 300 m, and 80 m, respectively. The juvenile components correspond to porphyritic andesitic rocks (Table 1) exhibiting a crystal assemblage including plagioclase, hornblende, biotite, opaque minerals, pyroxenes, and quartz. Disequilibrium mineral textures, such as resorption zones and reaction rims formed by plagioclase, magnetite, and orthopyroxene, have been reported (Arnosio, 2010; Fig. 3c). The juvenile clasts may also contain dark-grey mafic inclusions (Fig. 2c) characterized by a

dyktitaxitic texture (Fig. 3d) and a crystalline assemblage composed of hornblende, plagioclase, and opaque minerals.

The rocks of the Cajon Unit are affected by the development of a hydrothermal system, which is exposed in the central sector of the volcanic edifice (Fig. 2d). The hydrothermal alteration developed in two discrete zones showing an alunite + illite + jarosite and alunite + illite mineral association, respectively (Bustos et al., 2021). In addition, an angular unconformity separates this unit from the Chimpa Unit (Fig. 2e; Bustos et al., 2020; Norini et al., 2020).

2.2.3. Chimpa Unit

The Chimpa Unit consists of a homogeneous succession of radially-distributed lava flows, covering a surface of approximately 32 km^2 (with thickness of 300-400 m). The lavas display blocky to foliated textures, and are petrographically and geochemically distinguished into three distinct types: mafic, intermediate, and felsic lavas (Table 1). Mafic lavas are porphyritic to glomeroporphyritic and contain olivine, clinopyroxene, plagioclase, opaque minerals, and quartz xenocrysts, all embedded in a glassy matrix (Table 1). Intermediate lavas are porphyritic and contain a mineral assemblage consisting of olivine, clinopyroxene, orthopyroxene, plagioclase, hornblende, biotite, opaque minerals, and quartz. On the other hand, plagioclase, hornblende, biotite, opaque minerals, clinopyroxene, and orthopyroxene phenocrysts compose the mineral assemblage of the felsic lavas (Fig. 3d). Disequilibrium textures such as clinopyroxene reaction rims on olivine and quartz (Fig. 3e), or plagioclase + orthopyroxene + magnetite reaction rims on hornblende and biotite, are commonly observed. Sparse mafic inclusions are reported within the lava flows, containing hornblende, plagioclase, and olivine crystals and a dyktitaxitic glassy groundmass.

3. Methods

Sample preparation and U-Pb age determinations on zircons were conducted at the LaTe Andes laboratory of Salta (Argentina) using a laser ablation multi-collector inductively coupled plasma mass spectrometry (LA-ICP-MS) equipped with a RESOlution 193 laser ablation (Australian Scientific Instruments) and 8900 triple quadrupole ICP-MS (Agilent Technologies). The zircon crystals were preliminarily extracted crushing approximately 2 kg of rock samples using elutriation and magnetic techniques, and then they were selected by optical observations. For the LA-ICP-MS analyses, the standard zircon 91500 and Plesovice samples were considered as the reference materials for calculating the zircon U-Pb ages (Wiedenbeck et al., 2004; Sláma et al., 2008) and, during the analyses, a spot size of 24 µm was selected. The data were then processed using the LARD (Norris Scientific), the Isoplot 4.15 (Ludwig, 2003), and IsoplotR (Vermeesch, 2018) software for the determination of the concordia ages.

4. Results

4.1. U-Pb dating

A total of two hundred and fifty-one U-Pb zircon ages were determined across three rock samples to constrain the temporal evolution of the Chimpa magmatic system (Supplementary Data, Table S1). One sample corresponds to a white pumice (sample PB 211) from the Basal Unit, the second to a juvenile component of the block-and ash-flow deposits from the Cajón Unit (sample CBYC 209), and the third corresponds to a lava flow from the Chimpa Unit (sample CL 207). The concordia ages are plotted with 2σ uncertainty ellipses, and discordia intercept ages are provided at 95% confidence (Supplementary Data, Table S1). The measured isotopic ratios and the calculated ages for the samples are displayed on conventional concordia plots (Wetherill) in Fig. 4a-c. Zircon crystals are abundant in all the analyzed samples, mainly exhibiting euhedral to subehdral shapes and prismatic habits of 150 - 300 µm

in length (Fig. 4d). Sparse, roundly-shaped crystals (Fig. 4d), apparently more abundant in the Basal and Cajon units, display xenocrystic ages of approximately 500-550 Ma (Supplementary Data, Table S1).

For the sample PB 211 (Basal Unit), thirty-four spot analyses yielded a concordia $^{206}Pb/^{238}U$ age of 7.512 ± 0.037 Ma (MSWD = 1.4; 95% confidence interval; Fig. 4a). For sample CBYC 209 (Cajón Unit; Fig. 4b) we obtained a concordia $^{206}Pb/^{238}U$ age of 6.989 ± 0.028 Ma (n = 28; MSWD = 0.96; 95% confidence interval). Finally, the sample CL207 (Chimpa Unit) yielded a concordia $^{206}Pb/^{238}U$ age of 7.359 ± 0.0071 Ma (n = 32; MSWD = 0.99; 95% confidence interval; Fig.4c).

4.2. Zircon chemistry

The Th and U contents, estimated during the U-Pb isotopic determinations, serve as a preliminary chemical characterization of the zircon populations from the Chimpa volcanic rocks (Fig. 5). Collectively, the U contents range between 52 and 4258 ppm (mean 920 ppm), and no systematic variation are observed across the different volcanic units (Fig. 5a; Supplementary Data, Table S1). A similar trend is true for the Th estimates (Fig. 5a), which vary between 33 and 8860 ppm (mean 885 ppm). The Th/U ratios span a relatively wide range (0.11-3.4), but most of the values are between approximately 0.1 and 2.0 (mean 0.82; Fig. 5b, c). A limited subset of zircon grains from the Cajon Unit (n = 3) reaches a Th/U values between ca. 2.5 and 3.5 (Supplementary Data, Table S1). Except for this, no systematic variation in the Th/U ratios are observed among the considered volcanic lithologies. The comparison with the zircon population from the proximal, late Miocene Ramadas rhyolitic rocks reveals some differences: i) the Ramadas zircon are generally more enriched in U than those from the Chimpa rocks at comparable Th contents (Fig. 5a-c), and (ii) the Th/U range of the rhyolitic zircon is narrower (Th/U < 1) than that of the Chimpa zircon grains (Fig. 5d). However,

overlapping compositions between the Chimpa and Ramadas volcanoes are observed when considering the low-Th (≤1000 ppm) and low-U (<5000 ppm) zircon grains at Th/U values < 1 (Fig. 5a). To note, for the Ramadas rocks, this composition distinguish families of less-evolved, magmatic zircon antecrystals (high Ti, low Hf, low Eu/Eu*) from those crystallized in the pre-eruptive melt (high U, high Hf, low Ti, high Eu/Eu*; Bardelli et al., 2021; Fig. 5).

5. Discussion

5.1. Temporal constraints on the Chimpa magmatic system

Arnosio (2002) initially estimated the eruption age of the Chimpa volcano (Basal Unit) to be around 12 Ma, basing on the Rb/Sr isochrones for whole-rock, plagioclase, and biotite composition. However, the new U-Pb ages presented in this study indicate a younger magmatic/volcanic age of approximately 7.5-7.0 Ma. The magmatic significance of the obtained age span is supported by (i) the concordant zircon populations determined for the considered volcanic units (Fig. 4) and (ii) the high Th/U ratios (>0.1) and euhedral shapes of the analyzed zircon crystals, both indicative of a magmatic origin (e.g., Belusova et al., 2002; Hartmann and Santos, 2004; Gagnevin et al., 2010; McKay et al., 2018). The overlapping compositions, at Th/U ratios <1, between the zircon population of the Chimpa and the Ramadas magmatic antecrystals (low Eu/Eu*) also supports the hypothesis of a magmatic origin (Fig. 5b). Conversely, the higher Th/U ratios (up to 3.4 Th/U) and Th contents (up to approximately 9000 ppm) of the “andesitic” zircon populations relatively to the rhyolitic counterparts (Fig. 5c) suggest zircon crystallization occurred at high magmatic temperatures from a poorly evolve melt (Xiang et al., 2011), and the Th enrichment may also be attributed to the absence of a co-crystallizing, Th-bearing mineral phase. This hypothesis of high magmatic temperatures aligns with the results obtained by the application of the amphibole-plagioclase thermometry, which indicates temperatures exceeding 800°C (Arnosio, 2002).

Yet, some discrepancies arise looking at the concordia age obtained for the zircon population of the Chimpa Unit (Fig. 4c) relatively to the volcanic sequence as reconstructed by Bustos et al. (2020). Indeed, this age (7.359 ± 0.07 Ma) is older than that of the preceding Cajon Unit (6.989 ± 0.028). Such a deviation suggests that this age might not accurately represent the third volcanic phase based on field relations (Arnosio, 2010; Bustos et al., 2020). This discrepancy could result by a process of pre-eruptive juxtaposition of accessory antecrysts within the erupting melt during segregation (e.g., Bacon and Lowenstern, 2005; Miller et al., 2007), raising by consequence the final concordia age of the zircon population. Antecrystic mineral phases are commonly transported in melts segregating from a crystal mush (e.g., Coira et al., 2018; Wang et al., 2007), a process that may be enhanced by magma injection events (e.g., Walker et al., 2013; Feng and Zhu, 2018). Significant evidence of magma mixing/mingling and recharge events (particularly for the Chimpa Unit), are observed in the Chimpa deposits as indicated by the presence of (i) banded textures in the rocks, (ii) mafic inclusions, (iii) disequilibrium mineral assemblages, and (iv) inversely-zoned and resorbed crystals (Arnosio, 2010). To further explore this hypothesis, we calculated the Fractionation Factor (FF) of the Chimpa zircon population in relation to their respective whole-rock analyses ($Th_{(zrnn/melt)}/U_{(zrn/melt)}$; Kirkland et al., 2015; Arnosio, 2002; Fig. 6). In the case of Ramadas, this parameter aided in distinguishing between antecrystic, and autocrystic zircon families (Fig. 6), representing different generations, melt compositions, and crystallization temperatures (Bardelli et al., 2021). As observed in Fig. 6, the Chimpa zircons exhibit FF values ranging 0.03-0.96, overlapping with both the Ramadas antecrysts and autocrysts populations. Based on this, it is possible to hypothesize that the obtained concordia ages (particularly for the Chimpa Unit) result from a mixed zircon association consisting of a heterogeneous zircon cargo (e.g., Miller et al., 2007; Wang et al., 2007; Klemetti and Clynne, 2014). In light of this, a detailed textural analysis through chatodoluminecience and a chemical characterization of the zircons are necessary to define more accurately the magmatic and volcanic timelines intrinsic to the

Chimpa evolution. In addition, confirming the presence of a pre-eruptive event of zircon crystallization (i.e., autocrysts) requires analyzing the zircon chemistry, particularly focusing on the Eu/Eu* and trace-element concentrations (Belusova et al., 2002; Zhong et al., 2018; Olierook et al., 2020). Indeed, if a true autocrystic zircon phase were not present, then the U-Pb concordia ages of the Chimpa zircons would be strictly related to the antecrystic component, being in this sense more representatives of the magmatic dynamics and composition of the mush reservoir rather than the pre-eruptive conditions of the melts. In such a scenario, it would be logical to infer that the lavas belonging to the last eruptive cycle (the Chimpa Unit) would be the most enriched in the antecrystic zircon component derived from the first two magmatic phases. By consequence, these lavas would exhibit a U-Pb zircon concordia age (7.359 ± 0.071 Ma) comparable to the average (~7.4 Ma) of those from the Basal (7.517 ± 0.037 Ma) and Cajon (6.989 ± 0.028 Ma) units.

Based on the discussion thus far, it is evident that undertaking a comprehensive chemical characterization of the Chimpa zircon population, combined with the presented U-Pb ages, is crucial for conducting a detailed investigation of the magmatic and volcanic connections. However, the zircon concordia ages of the Basal and Cajon units appear to be consistent estimates, although preliminary, of the timing for the Chimpa magmatism. This allows considering the temporal evolution of this stratovolcano in the U-Pb chronostratigraphic framework of the APVC and northern Puna volcanic rocks. Furthermore, the geographical (and temporal) association of the Chimpa volcano with the rhyolitic Ramadas Volcanic Center and other volcanic rocks in the surroundings (Fig. 1b) provides an opportunity to explore the magmatic evolution of this specific sector of northern Puna during the Late Miocene, at the boundary between the Puna plateau and the Eastern Cordillera domains (Fig. 1b).

5.2. The Chimpa magmatism in the geochronological context of the APVC and northern Puna

The U-Pb zircon ages discussed thus far indicate that the Chimpa magmatic system was active from ca. 7.5 to <7.0 Ma, fairly coinciding with the regional period of low-flux magmatism separating the first two pulses of flare-up in the APVC (Kern et al., 2016; DeCelles et al., 2015; Fig. 7). The steady-state character of the Chimpa volcanism is consistent with the whole-rock geochemistry of the volcanic products (predominant andesitic composition) and the shield-like morphology of the volcanic edifice (Arnosio, 2010; Norini et al., 2013; Wörner et al., 2018; Bustos et al., 2022; Fig. 2a). As previously discussed, uncertainties remain regarding the exact age for the Chimpa Unit rocks. However, these rocks are younger than ca. 7.0 Ma (The Cajon Unit; Fig. 4b), postdating the development of the local hydrothermal system affecting the Cajon rocks (Bustos et al., 2021; Fig. 2d). This time lapse could be in the order of ca. 10^5-10^6 years, as inferred for the duration of hydrothermal systems related to stratovolcanoes in Central Andes and worldwide (e.g., Sillitoe, 2010; John et al., 2019; Pan et al., 2019). Furthermore, an evident temporal gap between the Cajon and Chimpa units is also highlighted by the angular unconformity separating these two volcanic phases (Fig. 2e).

Regardless the exact age of the Chimpa Unit, the presence of magma in this particular sector of the Puna plateau at ca. 7.5-7.0 Ma coincides with the period of maximum volcanic activity in the back-arc region (Late Miocene to Quaternary; e.g., Matteini et al., 2002; Petrinovic et al., 1999, 2005; Mazzuoli et al., 2008). Particularly, the present U-Pb ages indicate simultaneity with the youngest volcanic events of the Las Burras-Almagro-El Toro magmatic complex (ca. 14-6 Ma) of the Eastern Cordillera, represented by the Almagro (7.4-6.4 Ma) volcanic members described by Mazzuoli et al. (2008). Both the Chimpa and Almagro rocks share some geochemical and petrographic affinities such as intermediate compositions and a dominant plagioclase + hornblende + pyroxene + olivine + opaque phenocryst association (Mazzuoli et al., 2008; Arnosio, 2010; Table 1). Given this petrographic relation, and based on the presented zircon U-Pb ages, we infer that contemporaneous pulses of mantle-derived magmas promoted the simultaneous development of the Chimpa and Almagro volcanic

systems both at the border of the Puna plateau and in the Eastern Cordillera, respectively. This geochronologic linkage may serve as a base for investigating the isotopic and geochemical characteristics of the Chimpa rocks, in order to define the possible petrogenetic affinities between the Chimpa and Almagro volcanic rocks. This, in turn, will help in understanding the geodynamic and petrogenetic processes active at the Puna/Eastern Cordillera border during the Late Miocene (e.g., Mazzuoli et al., 2008).

Adjacent to the Chimpa volcano within the plateau, the rhyolitic Ramadas Volcanic Center developed on the opposite side of the thrust-bounded San Antonio de los Cobres graben (Fig. 1b; Viramonte et al., 1984; Norini et al., 2013). For the Ramadas rocks, geochronologic and stratigraphic evidence indicate the presence of a long-lived magmatic system characterized by events of magmatism (presence of melt, segregation of highly evolved rhyolites) in an upper-crustal mush reservoir (1-1.5 kbar), during (at least) two cycles, at ca. 9-8.7 Ma and at ca. 6.6-6.5 Ma, respectively (Coira et al., 2018; Lucci et al., 2018; Bardelli et al., 2021, and references therein). In the vicinity, during the magmatic lull separating these two magmatic phases, the Chimpa magmatic system developed (Fig. 7), fed by poorly evolved magmas in the shallowest portions of the crust, as testified by the common presence of mafic enclaves and banded rocks (Fig. 2c; Arnosio, 2010). The waning phase in the Ramadas reservoir (lack of zircon crystallization) suggests null or negligible inputs of magmas from the APMB region reaching the surface. It is worth noting that the Ramadas deposits lack mafic enclaves and banded textures (Bardelli et al., 2021). This indicates that the local APMB reservoir beneath the Chimpa and Ramadas volcanic centers showed a complex behavior during this period, resulting in volcanic products fairly close in time but with different degrees of evolution. In the case of the Chimpa rocks, the predominant andesitic composition suggests low fractionation degrees and relatively high ascension rates (Lucci et al., 2020; Maro et al., 2017). This observation, together with the petrographic and textural features of the Chimpa rocks, suggests that the deep APMB region here was not acting as a rheological barrier for the magmas raising from the

deep crust, a scenario also consistent with a peripheral position relatively to the center of the APMB anomaly (e.g., Walker et al., 2013; Maro et al., 2017; Fig. 1). On the contrary, the lack of mafic enclaves in the Ramadas rocks suggests that the APMB region was hindering the mafic magmas from ascending towards the surface, favoring instead magma differentiation through crystallization and/or interaction with the crustal lithologies (e.g., Caffe et al., 2002; Burns et al., 2015; Coira et al., 2018). Such a context highlights the occurrence, at a local scale and at comparable times, of complex dynamics of magma genesis in the middle- and upper-crustal reservoirs. A heterogeneous rheological structure in the crust, both considering the basement lithologies and the crystalline material accumulated during previous magmatic stages, may contribute to the geochemical variability of the related volcanic products, favoring, or alternatively contrasting, the ascent of mafic magmas towards the surface (e.g., Walker et al., 2013; Burns et al., 2015). In such a context, it appears that an extensive geochronologic characterization of the volcanic rocks of such complex volcanic regions is necessary to comprehend the magmatic evolution and processes active at both local and regional scales.

6. Conclusions and final remarks

The U-Pb zircon data presented in this study provide insights into the magmatic evolution of the Chimpa volcano of northern Puna. The main conclusions can be summarized as follows:

(i) The zircon association of the considered volcanic rocks exhibits Th/U values (0.11-0.34), Th contents (33-8860 ppm), and external morphologies (dominant euedral habits) coherent with a magmatic crystallization from poorly evolved magmas at high temperatures (>800°C).

(ii) Certain discrepancies between the U-Pb zircon ages and the stratigraphic relations of the volcanic lithologies can be attributed to the juxtaposition of accessory antecrysts in the erupting melts. Particularly, the last volcanic cycle (the Chimpa Unit) may have been

significantly affected by the presence of antecrystic zircons derived from the two previous magmatic stages (Basal and Cajon units).

(iii) The obtained U-Pb ages indicate that the Chimpa volcanic system developed from ca. 7.5 to <7.0 Ma, coinciding with a regional, steady-state magmatic phase dividing the first two pulses of ignimbritic flare-up in the APVC.

(iv) The close temporal relationship observed at a local scale with the rhyolitic Ramadas Volcanic Center (Puna plateau) and the andesitic to dacitic Almagro volcanic rocks (Eastern Cordillera) suggests that, in this particular sector of the Central Andes, the magma plumbing system showed complex behavior, leading to the generation of melts with variable geochemical compositions and eruptive styles at similar times.

Further geochemical studies considering the zircon populations the Chimpa volcano are essential for a deeper understanding of the magmatic and volcanic connection and to constrain more precisely the exact duration of the magmatic system. This in turn will help to understand, in combination with the geochemical and isotopic characterization of the Chimpa rocks, the petrogenetic dynamics active in this sector of the APMB during the Late Miocene, at the boundary between the northern Puna plateau and the Eastern Cordillera domains.

Acknowledgments

Financial support was given by PICT 2017 0351 grant to EB and 1978/1 CIUNSa grant to MA. U-Pb resulted by the agreement between CONICET and LaTe Andes laboratory. The constructive comments of two anonymous reviewers as well as the professional handling of Editor, Prof. Sanzhong Li greatly contributed to improve the manuscript. Authors warmly thank Prof. M. Santosh. LB thanks F. Lucci for the interesting discussion about the timing of the Altiplano-Puna magmatism.

References

Aceñolaza, F., Aceñolaza, G. (2005). La Formación Puncoviscana y unidades estratigráficas vinculadas en el Neoproterozoico-Cámbrico temprano del Noroeste Argentino. Latin American Journal of Sedimentology and basin analysis, 12(2), 65-87.

Acocella, V., A. Gioncada, R. Omarini, U. Riller, R. Mazzuoli, L. Vezzoli (2011), Tectonomagmatic characteristics of the back-arc portion of the Calama–Olacapato–El Toro Fault Zone, Central Andes, Tectonics, 30, TC3005, doi:10.1029/2010TC002854.

Allmendinger, R. W., Ramos, V. A., Jordan, T. E., Palma, M., Isacks, B. L. (1983). Paleogeography and Andean structural geometry, northwest Argentina. Tectonics, 2(1), 1-16.

Alonso, R., Viramonte, J., Gutierrez, R. (1984). Puna Austral. Bases para el subprovincialismo geológico de la Puna argentina. In Congreso Geológico Argentino (No. 9, pp. 43-63).

Arnosio, J. M. (2002). Volcanismo, geoquímica y petrología del volcán Chimpa (24 LS–66 LO) provincia de Salta, República Argentina. Ph.D. Thesis, Universidad Nacional de Salta, Salta, Argentina

Arnosio, M. (2010). Evidencia textural y geoquímica de mezcla de magmas en el volcán Chimpa, Puna Salteña. Revista de la Asociación Geológica Argentina, 66(1-2), 253-270.

Bacon, C.R., Lowenstern, J.B. (2005). Late Pleistocene granodiorite source for recycled zircon and phenocrysts in rhyodacite lava at Crater Lake, Oregon. Earth and Planetary Science Letters 233, 277–293

Balaram, V., Rahaman, W., & Roy, P. (2022). Recent advances in MC-ICP-MS applications in Earth and environmental sciences: Challenges and solutions. Geosystems and Geoenvironment, 1(2), 100019. https://doi.org/10.1016/j.geogeo.2021.100019

Bardelli, L., Becchio, R., Ortíz, A., Schmitt, A. K., Pereira, R., Báez, W., .Giordano, G. (2021). Repeated extraction of aphyric melts in a rhyolitic system revealed by zircon age and composition: The Ramadas Volcanic Centre (Puna plateau), NW Argentina. Lithos, 392, 106141. https://doi.org/10.1016/j.lithos.2021.106141

Belousova, E. A., Griffin, W. L., O'Reilly, S. Y., Fisher, N. L. (2002). Igneous zircon: trace element composition as an indicator of source rock type. Contributions to mineralogy and petrology, 143, 602-622.

Burns, D. H., de Silva, S. L., Tepley III, F., Schmitt, A. K., Loewen, M. W. (2015). Recording the transition from flare-up to steady-state arc magmatism at the Purico–Chascon volcanic complex, northern Chile. Earth and Planetary Science Letters, 422, 75-86.

Bustos, E., Arnosio, M., Báez, W., Norini, G., Suzaño, N. O., Viramonte, J. G. (2020). Geomorphological evolution of the Chimpa stratovolcano in the back-arc region of the Central Andes. Geomorphology, 364, 107251. https://doi.org/10.1016/j.geomorph.2020.107251

Bustos, E., Simón, V., Arnosio, M., Norini, G., Ducart, D. F., Suzaño, N. (2021). The hydrothermal system associated with Miocene Chimpa volcano, Central Andes. Implications on potential mineralization. Journal of South American Earth Sciences, 105, 102998.

Bustos, E., Capra, L., Arnosio, M., Norini, G. (2022). Volcanic debris avalanche transport and emplacement at Chimpa volcano (Central Puna, Argentina): Insights from morphology, grain-size and clast surficial textures. Journal of Volcanology and Geothermal Research, 432, 107671. https://doi.org/10.1016/j.jvolgeores.2022.107671

Caffe, P. J., Trumbull, R. B., Coira, B. L., Romer, R. L. (2002). Petrogenesis of Early Neogene magmatism in the Northern Puna; implications for magma genesis and crustal processes in the Central Andean Plateau. Journal of Petrology, 43(5), 907-942.

Chakraborty, P. P., Sharma, R., Das, K., Sharma, A., & Saha, S. (2023). U-Pb zircon geochronology of volcaniclastics and encasing sandstones from the Chhoti Khatu section: Bearing on the Neoproterozoic Marwar Supergroup stratigraphy and its global implications. Geosystems and Geoenvironment, 2(1), 100111. https://doi.org/10.1016/j.geogeo.2022.100111

Chmielowski, J., Zandt, G., Haberland, C. (1999). The central Andean Altiplano-Puna magma body. Geophysical Research Letters, 26(6), 783-786.

Coira, B., Kay, S. M., Viramonte, J. (1993). Upper Cenozoic magmatic evolution of the Argentine Puna—A model for changing subduction geometry. International Geology Review, 35(8), 677-720.

Coira, B., Kay, S. M., Viramonte, J. G., Kay, R. W., Galli, C. (2018). Origin of late Miocene peraluminous Mn-rich garnet-bearing rhyolitic ashes in the Andean Foreland (Northern Argentina). Journal of Volcanology and Geothermal Research, 364, 20-34.

Coira, B. L., Cisterna, C. E., (2021). Ordovician Volcanism in the Puna. Textures, Structures and Processes of Volcanic Successions: Examples from Southern Central Andes (Northwestern Argentina, 22º–28ºS), 129-147.

de Silva, S.L. (1989). Altiplano–Puna volcanic complex of the central Andes. Geology 17, 1102–1106.

de Silva, S. L., Riggs, N. R., Barth, A. P. (2015). Quickening the pulse: fractal tempos in continental arc magmatism. Elements, 11(2), 113-118.

de Silva, S. L., Kay, S. M. (2018). Turning up the heat: high-flux magmatism in the Central Andes. Elements: An International Magazine of Mineralogy, Geochemistry, and Petrology, 14(4), 245-250.

DeCelles, P.G., Ducea, M.N., Kapp, P., Zandt, G. (2009). Cyclicity in Cordilleran orogenic systems. Nat. Geosci. 2, 251–257.

del Papa, C. E., Petrinovic, I. A. (2017). The development of miocene extensional and short-lived basin in the Andean broken foreland: The Conglomerado Los Patos, Northwestern Argentina. Journal of South American Earth Sciences, 73, 191-201.

Escuder-Viruete, J., Molina, E. A., Chinchilla, D., Gabites, J., Seggiaro, R., Marquetti, C. A., Heredia, N. (2022). Structural and temporal relationships between volcanic activity, hydrothermal alteration, epithermal Ag–Pb–Zn mineralization and regional stress regime in the Quevar Volcanic Complex (Puna plateau, Salta Province, NW Argentina). Journal of Structural Geology, 158, 104582.

Feng, W., Zhu, Y. (2018). Decoding magma storage and pre-eruptive processes in the plumbing system beneath early Carboniferous arc volcanoes of southwestern Tianshan, Northwest China. Lithos, 322, 362-375.

Gagnevin, D., Daly, J. S., Kronz, A. (2010). Zircon texture and chemical composition as a guide to magmatic processes and mixing in a granitic environment and coeval volcanic system. Contributions to Mineralogy and Petrology, 159, 579-596.

Giordano, G., Pinton, A., Cianfarra, P., Baez, W., Chiodi, A., Viramonte, J., Groppelli, G. (2013). Structural control on geothermal circulation in the Cerro Tuzgle–Tocomar geothermal volcanic area (Puna plateau, Argentina). Journal of Volcanology and Geothermal Research, 249, 77-94.

Hartmann, L. A., Santos, J. O. S. (2004). Predominance of high Th/U, magmatic zircon in Brazilian Shield sandstones. Geology, 32(1), 73-76.

Hildreth, W., Moorbath, S. (1988). Crustal contributions to arc magmatism in the Andes of central Chile. Contributions to mineralogy and petrology, 98(4), 455-489.

Hongn, F.D., Tubia, J.M., Aranguren, A., Mon, R. (2002). La monzodiorita de las Burras: un pluton miocenico con el batolito de Tastil, Cordillera Oriental Argentina, 15th, v.2, p. 128-133.

James, D. E. (1971). Plate tectonic model for the evolution of the Central Andes. Geological Society of America Bulletin, 82(12), 3325-3346.

John, D. A., Lee, R. G., Breit, G. N., Dilles, J. H., Calvert, A. T., Muffler, L. P., Clynne, M. A. (2019). Pleistocene hydrothermal activity on Brokeoff volcano and in the Maidu volcanic center, Lassen Peak area, northeast California: Evolution of magmatic-hydrothermal systems on stratovolcanoes. Geosphere, 15(3), 946-982.

Kern, J. M., de Silva, S. L., Schmitt, A. K., Kaiser, J. F., Iriarte, A. R., Economos, R. (2016). Geochronological imaging of an episodically constructed subvolcanic batholith: U-Pb in zircon chronochemistry of the Altiplano-Puna Volcanic Complex of the Central Andes. Geosphere, 12(4), 1054-1077. https://doi.org/10.1130/GES01258.1

Kirkland, C. L., Smithies, R. H., Taylor, R. J. M., Evans, N., McDonald, B. (2015). Zircon Th/U ratios in magmatic environs. Lithos, 212, 397-414.

Klemetti, E. W., Clynne, M. A. (2014). Localized rejuvenation of a crystal mush recorded in zircon temporal and compositional variation at the Lassen Volcanic Center, Northern California. PloS one, 9(12), e113157.

Lindsay, J. M., Schmitt, A. K., Trumbull, R. B., De Silva, S. L., Siebel, W., Emmermann, R. (2001). Magmatic evolution of the La Pacana caldera system, Central Andes, Chile: Compositional variation of two cogenetic, large-volume felsic ignimbrites. Journal of Petrology, 42(3), 459-486.

Lucci, F., Rossetti, F., Becchio, R., Theye, T., Gerdes, A., Opitz, J., Giordano, G. (2018). Magmatic Mn-rich garnets in volcanic settings: Age and longevity of the magmatic plumbing system of the Miocene Ramadas volcanism (NW Argentina). Lithos, 322, 238-249. https://doi.org/10.1016/j.lithos.2018.10.016

Lucci, F., Carrasco-Núñez, G., Rossetti, F., Theye, T., White, J. C., Urbani, S., ... Giordano, G. (2020). Anatomy of the magmatic plumbing system of Los Humeros Caldera (Mexico): implications for geothermal systems. Solid Earth, 11(1), 125-159.

Ludwig, K. R. (2003). User's Manual for Isoplot 3.00. Manual. Berkeley Geochronology Center: Berkeley, CA.

Maro, G., Caffe, P. J., Romer, R. L., Trumbull, R. B. (2017). Neogene mafic magmatism in the northern Puna Plateau, Argentina: Generation and evolution of a back-arc volcanic suite. Journal of Petrology, 58(8), 1591-1617.

Matteini, M., Mazzuoli, R., Omarini, R., Cas, R., Maas, R. (2002). The geochemical variations of the upper Cenozoic volcanism along the Calama–Olacapato–El Toro transversal fault system in the Central Andes (24°S): petrogenetic and geodynamic implications. Tectonophysics 345: 211-227

Mazzuoli, R., Vezzoli, L., Omarini, R., Acocella, V., Gioncada, A., Matteini, M., ... Scaillet, S. (2008). Miocene magmatism and tectonics of the easternmost sector of the Calama–Olacapato–El Toro fault system in Central Andes at~ 24 S: Insights into the evolution of the Eastern Cordillera. Geological Society of America Bulletin, 120(11-12), 1493-1517.

McKay, M. P., Jackson Jr, W. T., Hessler, A. M. (2018). Tectonic stress regime recorded by zircon Th/U. Gondwana Research, 57, 1-9.

Miller, J. S., Matzel, J. E., Miller, C. F., Burgess, S. D., Miller, R. B. (2007). Zircon growth and recycling during the assembly of large, composite arc plutons. Journal of Volcanology and Geothermal Research, 167(1-4), 282-299.

Norini, G., Baez, W., Becchio, R., Viramonte, J., Giordano, G., Arnosio, M., Groppelli, G. (2013). The Calama–Olacapato–El Toro fault system in the Puna Plateau, Central Andes: geodynamic implications and stratovolcanoes emplacement. Tectonophysics, 608, 1280-1297.

Norini, G., Bustos, E., Arnosio, M., Baez, W., Zuluaga, M. C., Roverato, M. (2020). Unusual volcanic instability and sector collapse configuration at Chimpa volcano, central Andes. Journal of Volcanology and Geothermal Research, 393, 106807.

Olierook, H. K., Kirkland, C. L., Szilas, K., Hollis, J. A., Gardiner, N. J., Steenfelt, A., ... & McDonald, B. J. (2020). Differentiating between inherited and autocrystic zircon in granitoids. Journal of Petrology, 61(8), egaa081.

Pan, J. Y., Ni, P., Chi, Z., Wang, W. B., Zeng, W. C., Xue, K. (2019). Alunite 40Ar/39Ar and zircon U-Pb constraints on the magmatic-hydrothermal history of the Zijinshan high-sulfidation epithermal Cu-Au deposit and the adjacent Luoboling porphyry Cu-Mo deposit, South China: implications for their genetic association. Economic Geology, 114(4), 667-695.https://doi.org/10.5382/econgeo.4658

Petrinovic, I. A., Mitjavila, J., Viramonte, J. G., Martí, J., Becchio, R., Arnosio, M., Colombo, F. (1999). Descripción geoquímica y geocronológica de secuencias volcánicas neógenas de Trasarco, en el extremo oriental de la Cadena Volcánica Transversal del Quevar (Noroeste de Argentina). Acta Geologica Hispanica, 1999, vol. 34, num. 2-3, p. 255-272.

Petrinovic, I. A., Riller, U., Brod, J. A. (2005). The Negra Muerta Volcanic Complex, southern Central Andes: geochemical characteristics and magmatic evolution of an episodically active volcanic centre. Journal of Volcanology and Geothermal Research, 140(4), 295-320.

Petrinovic, I. A., Riller, U., Brod, J. A., Alvarado, G., Arnosio, M. (2006). Bimodal volcanism in a tectonic transfer zone: evidence for tectonically controlled magmatism in the southern Central Andes, NW Argentina. Journal of Volcanology and Geothermal Research, 152(3-4), 240-252.

Petrinovic, I. A., Martí, J., Aguirre-Diaz, G. J., Guzmán, S., Geyer, A., Paz, N. S. (2010). The Cerro Aguas Calientes caldera, NW Argentina: an example of a tectonically controlled, polygenetic collapse caldera, and its regional significance. Journal of Volcanology and Geothermal Research, 194(1-3), 15-26.

Ramos, V. A., (1970). Geología de los primeros contrafuertes de la Puna Salto-Jujueña entre San Antonio de los Cobres y El Moreno. Ph.D. Thesis, Universidad de Buenos Aires, Argentina.

Ramos, V. A., (1973). Estructura de los primeros contrafuertes de la Puna Salto-Jujueña y sus manifestaciones volcánicas asociadas. 5th Congreso Geológico Argentino, Buenos Aires, Argentina. Actas (IV), 159–202.

Robl, K., Brodtkorb, M.K.D., Ametrano, S. (2009). La mineralización epitermal miocena del complejo estratovolcánico Quevar, Salta: Parte 1: Geología y petrología. Parte 2: La mineralización. Revista de la Asociación Geológica Argentina 64(3): 525-539

Salfity, J. A. (1985). Lineamentos transversales al rumbo andino en el Noroeste Argentino. In IV Congreso Geologico Chileno (Vol. 2, pp. 119-137). Antofagasta: Universidad del Norte Chile.

Schmitt, A.K., Lindasy, J.M., de Silva, S.L., Trumbull, R. (2002). U-Pb zircon chronostratigraphy of early-Pliocene ignimbrites from La Pacana, north Chile: implications for the formation of stratified magma chambers. J. Volcanol. Geotherm. Res. 120, 43–53. https://doi.org/10.1016/S0377-0273(02)00359-1

Sillitoe, R. H. (2010). Porphyry copper systems. Economic geology, 105(1), 3-41.

Sláma, J., Košler, J., Condon, D. J., Crowley, J. L., Gerdes, A., Hanchar, J. M., Schaltegger, U. (2008). Plešovice zircon—a new natural reference material for U–Pb and Hf isotopic microanalysis. Chemical Geology, 249(1-2), 1-35.

Turner, J.C.M. (1964). Descripción de la Hoja Geológica 7c, Nevado de Cachi, Salta. Technical report. Dirección Nacional de Geología y Minería, Boletín N 99.

Vermeesch, P. (2018). IsoplotR: A free and open toolbox for geochronology. Geoscience Frontiers, 9(5), 1479-1493.

Viramonte, J.G., Galliski, M.A., Araña Saavedra, V., Aparício, A., García Cucho, L., Martín Escorza, C. (1984). El finivulcanismo básico de la depresión de Arizaro, provincia de Salta. 9th Congreso Geológico Argentino. Actas (3), 234–251 Bariloche.

Walker, B.A., Klemetti, E.W., Grunder, A.L., Dilles, J.H., Tepley, F.J., Giles, D. (2013). Crystal reaming during the assembly, maturation, and waning of an eleven-million-year crustal magma cycle: thermobarometry of the Aucanquilcha Volcanic Cluster. Contribution to Mineralogy and Petrology 165, 663-682. https://doi.org/10.1007/s00410-012-0829-2

Wang, X., Griffin, W.L., O'Reilly, S.Y., Li, W. (2007). Three stages of zircon growth in magmatic rocks from the Pingtan Complex, Eastern China. Acta Geol. Sin. 81 (1), 68–80.

Ward, K. M., Zandt, G., Beck, S. L., Christensen, D. H., McFarlin, H. (2014). Seismic imaging of the magmatic underpinnings beneath the Altiplano-Puna volcanic complex from the joint inversion of surface wave dispersion and receiver functions. Earth and Planetary Science Letters, 404, 43-53.

Wiedenbeck, M., Hanchar, J. M., Peck, W. H., Sylvester, P., Valley, J., Whitehouse, M.,. Franchi, I. (2004). Further characterisation of the 91500 zircon crystal. Geostandards and Geoanalytical Research, 28(1), 9-39.

Wörner, G., Mamani, M., Blum-Oeste, M. (2018). Magmatism in the Central Andes. Elements 14 (4), 237–244. https://doi.org/10.2138/gselements.14.4.237

Xiang, W., Griffin, W. L., Jie, C., Pinyun, H., Xiang, L. I. (2011). U and Th contents and Th/U ratios of zircon in felsic and mafic magmatic rocks: Improved zircon-melt distribution coefficients. Acta Geologica Sinica-English Edition, 85(1), 164-174.

Zandt, G., Leidig, M., Chmielowski, J., Baumont, D., Yuan, X. (2003). Seismic detection and characterization of the Altiplano-Puna magma body, central Andes. Pure and Applied Geophysics, 160(3), 789-807.

Table Caption

Table 1 Petrographic characteristics from Chimpa volcano units.

Unit	Texture	Phenocryst assemblage	Matrix/Groundmass
Basal Unit White pumice	Porphyritic	**Plagioclase** (37% modal; <0.4 mm; euhedral and subhedral, zoned) + **Biotite** (34% modal; 0.3-1 mm; subhedral) + **Hornblende** (22% modal; also as a microphenocryst 0.1-0.6 mm; biotite inclusions) ± Quartz (4% modal; 0.3-0.7 mm; anhedral; rounded and embayed) ± Opaque (3% modal; as aggregates or as subhedral to anhedral isolated crystals) ± Orthopyroxene (euhedral; hornblende rim)	Glassy matrix, spheroidal to subspheroidal vesicles.
Basal Unit Gray Pumice	Porphyritic	**Hornblende** (49.5% modal; <1 mm; euhedral-subhedral; opaque inclusions) + **Biotite** (38.5% modal; <1 mm; subhedral; opaques inclusions) + **Plagioclase** (10% modal; <1 mm; glassy inclusions) + **Opaque** (2% modal; as magnetite and ilmenite; <1 mm; exsolution lamellae) ± augite and enstatite (<<0.5% modal; hornblende rim)	Glassy matrix, spheroidal to subspheroidal vesicles.
Cajón Unit Lithic in block-and-ash flow deposit	Porphyritic	**Plagioclase** (60% modal; 4-10 mm; microphenocryst <2 mm; subhedral and euhedral; glassy, hornblende and biotite inclusions) + **Hornblende** (24%; <2 mm; subhedral- euhedral) + **Biotite** (6% modal; 1.5 mm; 0.3-1 mm; plagioclase, magnetite and orthopyroxene as rim) + **Opaque** (4% modal; magnetite and ilmenite; as aggregates or as subhedral to anhedral isolated crystals) + **Clino and orthopyroxene** (4% modal; as aggregates with subhedral to anhedral crystals and also as isolated subhedral crystals <0.5 mm; magnetite inclusions) + **Quartz** (2% modal; anhedral; embayed).	Glassy to hialopilitic groundmass with plagioclase, hornblende, orthopyroxene and opaques microliths.
Cajón Unit Mafic inclusions in lithics from block-and-ash flow	Diktitaxitic	**Hornblende** (57% modal; <2 mm; acicular; secondarily euhedral to subhedral prismatic crystals) + **Plagioclase** (36% modal; <0.5 mm; elongated laths; glassy, opaque and hornblende inclusions) + **Opaque** (7% modal; 0.1 mm isolated crystals; 0.3 mm in aggregates; magnetite) ± Olivine (orthopyroxene rim) ± Clino and orthopyroxene (as aggregates with hornblende rim) ± Plagioclase xenocrysts (1.2 - 4.3 mm; resorption feature with limpid overgrowth)	Glassy and vesiculated groundmass (43% volume)
Chimpa Unit Mafic Lavas	Porphyritic	**Olivine** (30% modal; 0.2-1.6 mm; subhedral to anhedral; partially altered to iddingsite; opaque inclusions) + **Clinopyroxene** (25% modal; subhedral; opaque inclusions; as component of rim) + **Plagioclase** (40% modal; 3-10 mm; euhedral and subhedral; sieve texture; resorption features) + **Opaque** (<5% modal;	Glassy matrix with plagioclase and magnetite microliths.

		<0.5mm; euhedral and subhedral) + **Quartz xenocrysts** (<3.5% modal; anhedral; clinopyroxene and glass rim)	
Chimpa Unit Intermediate Lava	Porphyritic	**Olivine** (1 to 20% modal; 0.2-1.6 mm; subhedral to anhedral; partially altered to iddingsite; opaques inclusions; clinopyroxene rim) + **Clinopyroxene** (8% modal; generally as aggregate; subhedral; opaque inclusions; as component of rim) + **Orthopyroxene** (6% modal; 1 mm; subhedral; opaque inclusions; clinopyroxene rim) + **Plagioclase** (60% modal; 3-10 mm; euhedral to subhedral; reaction textures as sieve and resorption) + **Hornblende** (7% modal; 2.2-0.6 mm; euhedral and subhedral; opaque and plagioclase inclusions; plagioclase+orthopyroxene+magnetite rim; clinopyroxene rim; clinopyroxene replacement) + **Biotite** (10% modal; 0.2-1.5 mm; subhedral; plagioclase and opaques inclusions; resorbed crystal or with plagioclase+orthopyroxene+magnetite rim) + **Opaque** (<5% modal; <0.5mm; euhedral and subhedral) + **Quartz** (<3.5% modal; anhedral; clinopyroxene and glass rim)	Plagioclase, clino and orthopyroxene microliths in scarce glass.
Chimpa Unit Felsic Lavas	Porphyritic	**Plagioclase** (60% modal; 3-10 mm as isolated or glomerocrysts; euhedral to subhedral; glassy, biotite and opaques inclusions; sieve texture) + **Hornblende** (20-25% modal; 2.2-0.6 mm; euhedral and subhedral; plagioclase + orthopyroxene + opaques rim) + **Biotite** (6% modal; 0.2-1.5 mm; tabular; opaques and plagioclase inclusions; resorbed crystal or with plagioclase + orthopyroxene + magnetite rim) + **Opaque** (<5% modal; <0.5 mm; euhedral and subhedral; as inclusions in mineral or as reaction rims in hornblende and biotite) + **Clinopyroxene** (2% modal; generally as aggregate; subhedral; opaque inclusions; as component of rims around olivine, orthopyroxene and quartz) + **Orthopyroxene** (2% modal; 1 mm; subhedral) ± olivine (<1% modal; 0.2-1.6 mm; subhedral to anhedral; iddingsite alteration; opaques inclusions; hornblende rim) + quartz (<3.5% modal; anhedral; clinopyroxene and glass rim)	Plagioclase, orthopyroxene, magnetite and hornblende microliths in the groundmass.
Chimpa Unit Mafic inclusions in lavas	Diktitaxitic	**Hornblende** (45% modal; <1.5 mm; acicular and prismatic; resorbed borders) + **Plagioclase** (30% modal; < 1mm; euhedral and subhedral laths) + **Olivine** (10% modal; <2 mm; iddingsite alteration; opaque inclusions; clinopyroxene or hornblende rim)+ Clinopyroxene (10% modal; <0.7 mm; subhedral; opaque inclusions; as aggregates, isolates crystals or as reaction rims in olivine, orthopyroxene or quartz) + opaques + plagioclase xenocrysts (5% modal; sieve	Glassy matrix with scarce vesiculation.

		texture) + quartz xenocrysts (clinopyroxene and hornblende rims)	

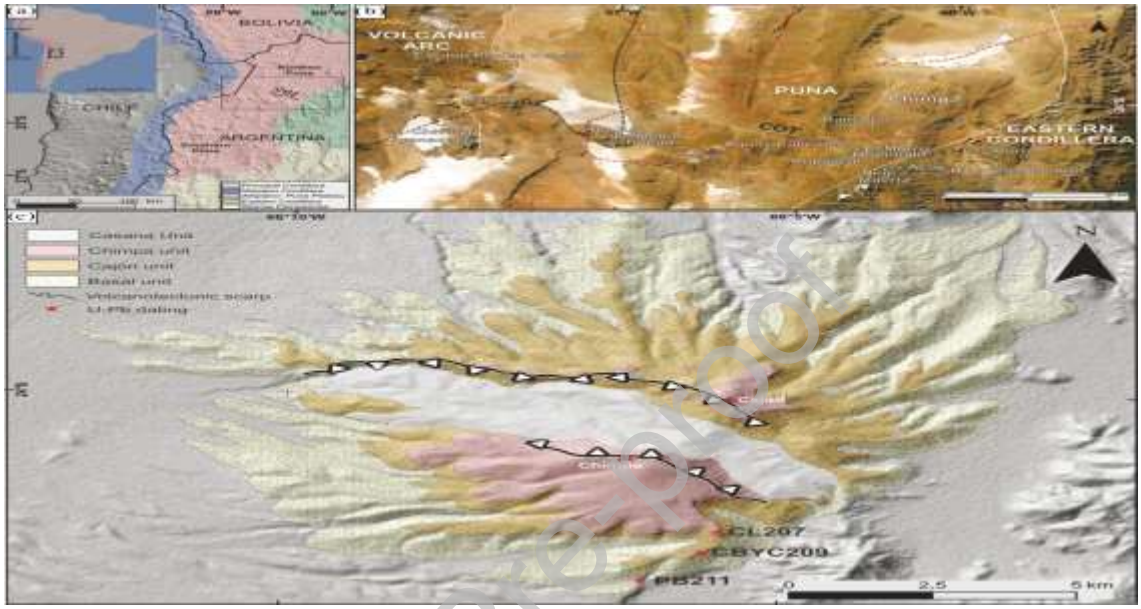

Figure Captions

Fig. 1. (a) Shaded SRTM DEM of the southern part of Central Andes with the major geological provinces. The inset in the upper left corner shows the location of the study area. (b) A satellite view of the Chimpa volcano in the eastern sector of the COT region. The location of the Miocene volcanic centers is indicated by green triangles (see the text for references). The dashed red lines mark the surface trace of the APMB geophysical anomaly (from Zandt et al., 2003), while the black dashed lines indicate the boundary inferred for the main APVC region (following Zandt et al., 2003). The boundaries between the Volcanic Arc, the Puna plateau and the Eastern Cordillera is highlighted by white lines. COT = Calama-Olacapato-El Toro fault

system. (c) Geological map of the Chimpa Volcano (modified after Bustos et al., 2022) with the location of the sampling sites.

Fig. 2. (a) Panoramic view of the Chimpa volcano. (b) Field view of the ignimbrite deposits from the Basal Unit. (c) Mafic inclusions in the andesitic lava from the Cajón Unit. d) Hydrothermal

alteration zone affecting the Basal and Cajón units. e) Angular unconformity (highlighted with a yellow line) between the Cajón and Chimpa units.

Fig. 3. Petrographic features of Chimpa units. (a) Microphotograph (cross-polarized lights) of white pumice (Basal Unit) showing quartz (Qtz), plagioclase (Pl) and biotite (Bt) phenocrysts. (b) Microphotograph (cross-polarized lights) of gray pumice (Basal Unit) showing high porphyricity, with plagioclase (Pl), biotite (Bt) and amphibole (Amp). (c) Microphotograph (cross-polarized lights) of a plagioclase (Pl) phenocryst with sieve oscillatory texture (Cajón Unit). (d) Microphotograph (cross-polarized lights) of a mafic inclusion from Cajón Unit showing dyktitaxitic texture. (Amp: amphibole; Px: pyroxene; Pl: plagioclase). (e) Microphotograph (cross-polarized lights) showing the association plagioclase (Pl) + pyroxene (Px) in the lava flows of Chimpa Unit. (f) Microphotograph (cross-polarized light) showing resorbed sub-rounded quartz (Qtz) rimmed by pyroxene (Px).

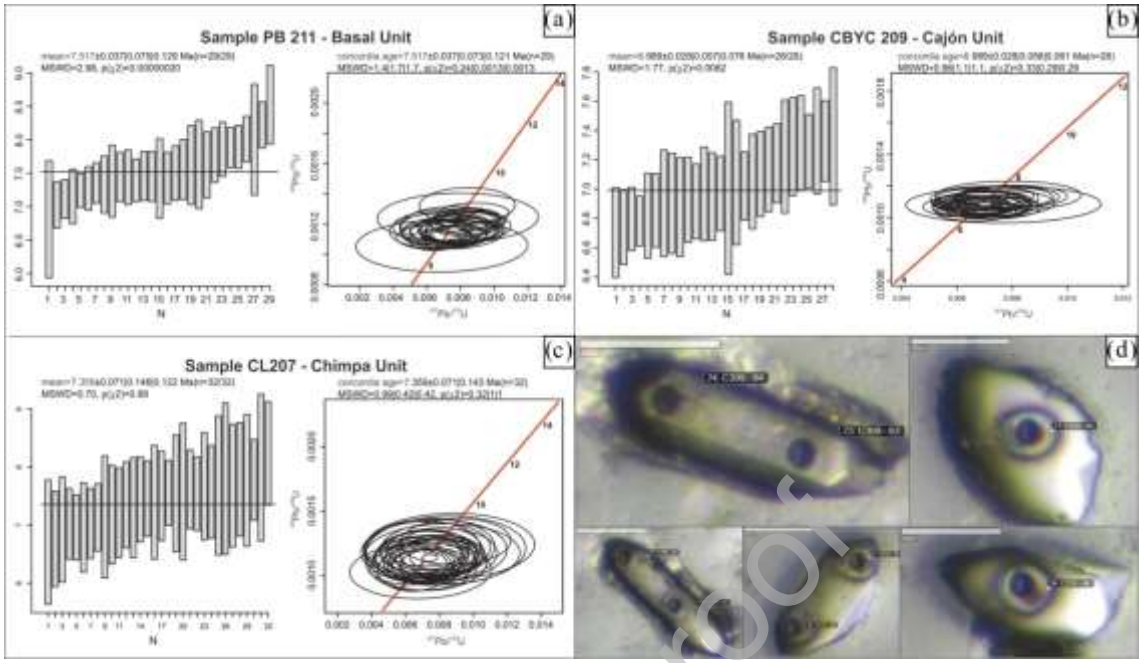

Fig. 4. U-Pb results obtained for the zircon crystals of the Chimpa volcanic rocks. (a-c) Confidence interval (left) and zircon U-Pb Concordia diagrams (right) of the analyzed samples. (a) Sample PB 211, Basal Unit. (b) Sample CBYC 209, Cajón Unit. (c) Sample CL207, Chimpa Unit. (d) Representative microphotographs of the analyzed zircon crystals.

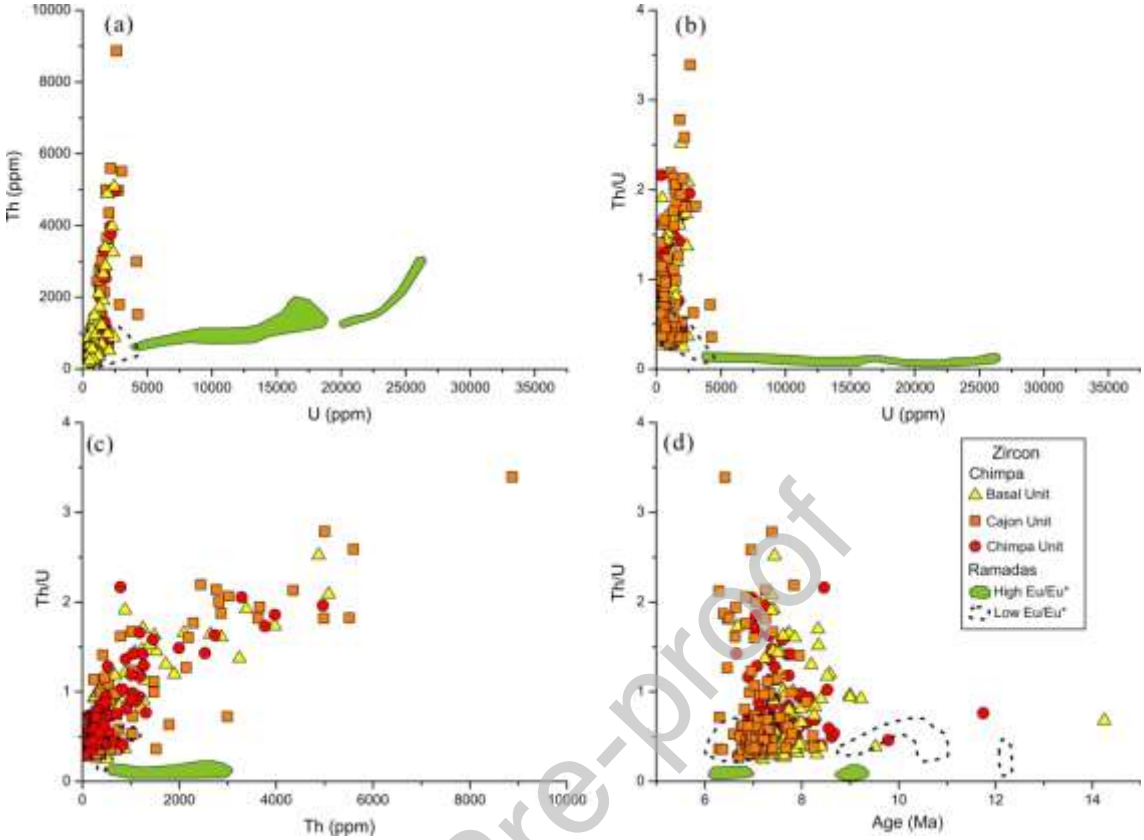

Fig. 5. Chemical characterization of the zircon crystals from the Chimpa volcanic rocks in the diagrams: (a) Th versus U; (b) Th/U ratio versus U; (c) Th/U ratio versus Th; (d) Th/U ratio versus age. The composition (and age) of the Ramadas rhyolitic zircon antecrysts (low Eu/Eu*) and autocrysts (high Eu/Eu*) is indicated by green areas and black dotted lines, respectively (data from Bardelli et al., 2021 and Lucci et al., 2018).

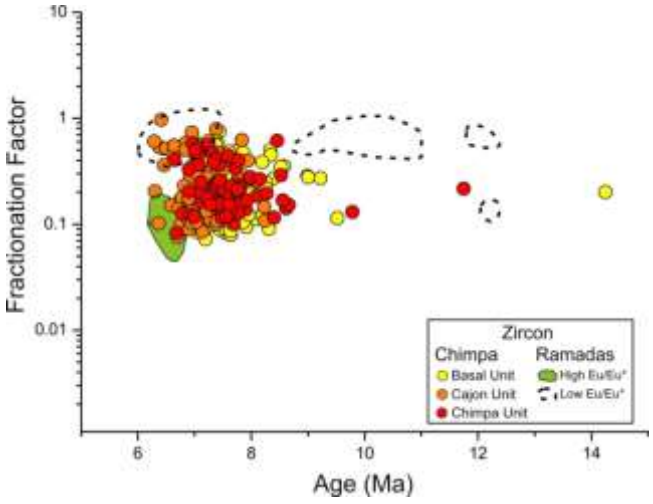

Fig. 6. The fractionation factor [$(Th_{zrn}/Th_{whole\text{-}rock})/U_{zrn}/U_{whole\text{-}rock}$) following Kirkland et al., 2015] versus the U-Pb age for the Chimpa and Ramadas zircon populations (Th and U whole-rock data from Arnosio, 2002). The data of the Ramadas magmatic antecrysts (Eu/Eu* = 0.11-0.51) and autocrysts (Eu/Eu* = 0.01-0.03) zircon crystals are from Bardelli et al. (2021).

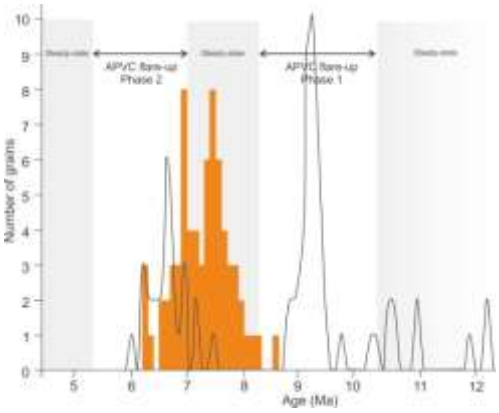

Fig. 7. Distribution of the U-Pb ages obtained for Chimpa Volcano (excluding xenocrysts) in the context of the APVC volcanic rocks (Kern et al., 2016). The black curve shows the frequency distribution of the U-Pb zircon ages obtained for the Ramadas Volcanic Center rocks (Bardelli et al., 2021).

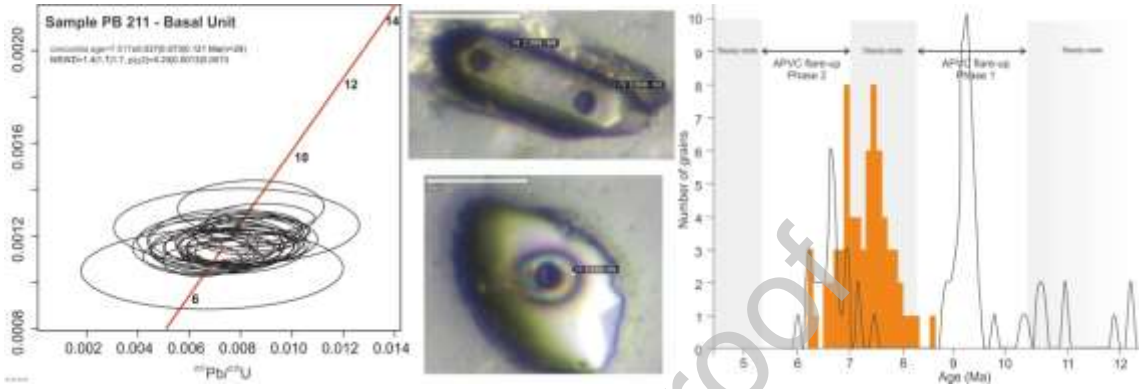

Graphical Abstract

Supplementary Data

Table S1 A total of two hundred and fifty-one U-Pb zircon ages were determined across three rock samples to constrain the temporal evolution of the Chimpa magmatic system.

CRediT authorship contribution statement

EM: Visualization; Data curation; Formal analysis; Funding acquisition; Investigation; Field work; Writing - original draft; Writing - review & editing. LB: Conceptualization; Writing - original draft; Writing - review & editing; Supervision. MA: Field work; Visualization; Funding acquisition; Investigation. RAB: Data curation; Visualization; Methodology; Investigation.

Declaration of interests

☒ The authors declare that they have no known competing financial interests or personal relationships that could have appeared to influence the work reported in this paper.

☐The authors declare the following financial interests/personal relationships which may be considered as potential competing interests: